Solid state NMR sequential resonance assignments and conformational analysis of the 2 × 10.4 kDa dimeric form of the *Bacillus subtilis* protein Crh

Anja Böckmann[a,*], Adam Lange[b], Anne Galinier[c], Sorin Luca[b], Nicolas Giraud[a], Michel Juy[a], Henrike Heise[b], Roland Montserret[a], François Penin[a] & Marc Baldus[b,*]
[a]*Institut de Biologie et Chimie des Protéines, C.N.R.S UMR 5086, 7, passage du Vercors, 69367 Lyon Cedex 07, France;* [b]*Max-Planck-Institute for Biophysical Chemistry, Solid-state NMR, Am Fassberg 11, 37077 Göttingen, Germany;* [c]*Institut de Biologie Structurale et Microbiologie, C.N.R.S UPR 9043, 31, chemin Joseph Aiguier, 13402 Marseille Cedex 20, France*

Abstract

Solid state NMR sample preparation and resonance assignments of the U-[^{13}C,^{15}N] 2 × 10.4 kDa dimeric form of the regulatory protein Crh in microcrystalline, PEG precipitated form are presented. Intra– and interresidue correlations using dipolar polarization transfer methods led to nearly complete sequential assignments of the protein, and to 88% of all ^{15}N, ^{13}C chemical shifts. For several residues, the resonance assignments differ significantly from those reported for the monomeric form analyzed by solution state NMR. Dihedral angles obtained from a TALOS-based statistical analysis suggest that the microcrystalline arrangement of Crh must be similar to the domain-swapped dimeric structure of a single crystal form recently solved using X-ray crystallography. For a limited number of protein residues, a remarkable doubling of the observed NMR resonances is observed indicative of local static or dynamic conformational disorder. Our study reports resonance assignments for the largest protein investigated by solid state NMR so far and describes the conformational dimeric variant of Crh with previously unknown chemical shifts.

Abbreviations: ssNMR – solid state NMR; MAS – magic angle spinning; Crh – catabolite repression histidine-containing phosphocarrier protein; HPr – histidine-containing phosphocarrier protein; CcpA – carbon control protein A; HprK/P – HPr kinase/phosphatase; PEG – polyethylene glycol; DSS – 2,2-dimethylsilapentane-5-sulfonic acid; CP – cross polarization; PDSD – proton driven spin diffusion; TPPM – two pulse phase modulation; RFDR – radio frequency-driven recoupling; DQ – double quantum; SPC-5 – supercycled POST-C5; r.f. radio frequency; HORROR – homonuclear rotary resonance; SPECIFIC-CP – spectrally induced filtering in combination with cross-polarization.

Introduction

Solid state NMR is rapidly developing to become complementary to liquid state NMR and X-ray crystallography as a method to study three-dimensional structure and dynamics in peptides and proteins. Because experiments can be conducted on insoluble and non-crystalline material, ssNMR is particularly well suited to investigate fibrous or membrane proteins at atomic resolution. In many cases, structural information regarding the complete polypeptide sequence is desirable making mandatory the application of tailored 2D ssNMR experiments in multiply labeled protein

*To whom correspondence should be addressed, E-mail: a.bockmann@ibcp.fr; E-mail: maba@mpibpc.mpg.de

variants. Examples in peptides (Straus et al., 1997; Hong and Griffin, 1998; Detken et al., 2001; Rienstra et al., 2002b; Petkova et al., 2002; Jaroniec et al., 2002), proteins (Straus et al., 1998; Hong, 1999; Tan et al., 1999; McDermott et al., 2000; Pauli et al., 2000, 2001, Böckmann and McDermott, 2002) and membrane proteins (Egorova-Zachernyuk et al., 2001; Creemers et al., 2002; Luca et al., 2003; Petkova et al., 2003) have been recently reported. As demonstrated in small peptides (Nomura et al., 1999; Rienstra et al., 2002a; Lange et al., 2003), and in a 63-residue protein (Castellani et al., 2002) these correlation experiments can be used to construct three-dimensional structures in the solid state. In general, solid-state NMR spectra directly report on the structural heterogeneity of the sample. Indeed, maximum spectral resolution is most easily achieved for samples showing high structural homogeneity. Adequate sample preparation is thus an important step for each protein study. Furthermore, experimental parameters such as the magic angle spinning rate, the amplitude of applied radio frequency irradiation and the sample temperature can affect sample stability and hence the 3D protein fold. Finally, the signal to noise ratio is of critical importance and may require expert optimization of the employed pulse sequences.

Extensive studies are currently underway in our laboratory to understand the structure-function relationship of the catabolite repression histidine-containing phosphocarrier protein (Crh). Crh has been found to date only in Gram-positive, spore-forming bacteria, such as *Bacillus subtilis* (Galinier et al., 1997, 1998). The specific function of Crh remains elusive (Deutscher et al., 2001). In contrast to its homologue HPr, it is not involved in sugar transport, since a Gln occupies position 15 instead of a His (Figure 1). Similar to HPr, Crh is phosphorylated by HprK/P on Ser 46, and was shown to interact with CcpA (Deutscher et al., 1995; Jones et al., 1997; Galinier et al., 1997, 1998). The resulting protein complexes, CcpA/P-Ser-HPr or CcpA/P-Ser-Crh, specifically interact with the catabolite response elements (*cre*) and regulate the expression of numerous genes (Stulke and Hillen, 2000).

Besides its biological relevance, Crh has been shown to exist in remarkably different conformations. In solution, Crh forms a mixture of monomers and dimers in a slowly (i.e., time scale of hours) exchanging equilibrium (Penin et al., 2001). NMR spectroscopy on Crh solutions containing monomers and dimers led to 3D structure determination of the monomer and enabled us to partially identify the dimer interface (Favier et al., 2002). Sequential assignments of the residues located in the dimer region were not possible using liquid state NMR methods due to the low intensity of the corresponding resonances and the tendency of the dimer to precipitate under all tested liquid state NMR conditions. Solid state NMR investigations on these precipitates indicated a partially unfolded protein state and were of limited use to gain insight into the Crh dimer structure. For this reason, we developed an original approach leading to Crh in microcrystalline and single-crystalline form. X-ray crystallography on Crh single crystals diffracted at 1.8 Å resolution and revealed a 3D domain swapped Crh dimer structure formed by β1-strand swapping of two monomers (Juy et al., 2003).

In this report we present the solid state NMR sample preparation and nearly complete ^{13}C and ^{15}N sequential assignments of a microcrystalline form of Crh. We show that most of the 85 residues can be readily assigned using 500 and 600 MHz NMR 2D spectroscopy at medium-size magic angle spinning (Andrew et al., 1958) rates. Our study allows for a structural comparison to Crh structures studied in the solution state (Favier et al., 2002) and as a single crystal form (Juy et al., 2003). Resonance assignments obtained in the solid state differ from NMR data obtained in the solution state for several protein segments. A subsequent prediction using TALOS (Cornilescu et al., 1999) led to backbone dihedral angles that are consistent with a microcrystalline dimeric form of Crh that closely resembles the single crystal structure. Chemical shift assignments are hence consistent with the investigation of a 85 × 2 residue dimer in the solid state. Finally, dynamic and/or static disorder has been detected for a restricted number of residues located mainly at the dimer interface. These observations could potentially be important for explaining the mechanism of domain swapping and for the interaction of Crh with other molecules.

Materials and methods

Sample preparation

Crh was overexpressed with a C-terminal LQ(6xHis) extension as described previously (Galinier et al., 1997). Uniformly [^{13}C,^{15}N] labeled Crh was obtained by growing bacteria in Silantes growth media. The protein was purified on Ni-NTA agarose (QUIAGEN)
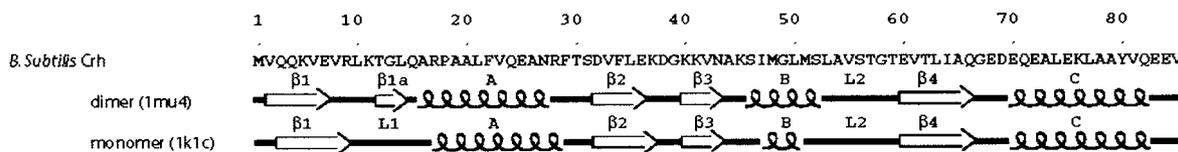
Figure 1. Amino acid sequence and secondary structure of the *Bacillus Subtilis* Crh dimer and monomer deduced from the 3D structures of PDB entries 1mu4 (Juy et al., 2003) and 1k1c, (Favier et al., 2002) respectively.

columns followed by anion exchange chromatography on a Resource Q column (Penin et al., 2001). Crh-containing fractions were dialyzed against 20 mM NH_4HCO_3.

We used 5–20 mg/ml protein concentrations as obtained after dialysis in sitting drops of 100–200 μl deposited on a siliconated crystallization glass plate or on siliconated cover slides in Linbro plates (Hampton). The same volume of a 20% solution of PEG 6000 and 0.02% NaN_3 in 20 mM NH_4HCO_3 was added to the drops, over 2 M NaCl reservoir solution. The plates were left at 4 °C until a precipitate appeared (1–2 weeks). Resulting microcrystals were directly centrifuged at 2000 *g* into 4 mm Bruker CRAMPS rotors and rotor caps were sealed with glue. The samples used in this study contained between 8 and 20 mg of protein.

NMR spectroscopy

NMR experiments were performed on Bruker AVANCE DSX 500 and 600 MHz wide bore spectrometers, both equipped with double (^{1}H, ^{13}C) and triple resonance (^{1}H, ^{13}C, ^{15}N) Bruker MAS probes, at spinning speeds of 10 and 11 kHz. All experiments were carried out at probe temperatures between -10 and -5 °C (corresponding to a sample temperature between 5–10 °C). A ramped cross-polarization (Metz et al., 1994; Hediger et al., 1995) was used in all experiments to transfer proton magnetization to the ^{13}C or ^{15}N spins. High power proton decoupling using the TPPM decoupling scheme (Bennett et al., 1995) was applied during evolution and detection periods. The relaxation delay between scans was either 2 or 3 s.

^{13}C *homonuclear spectroscopy.* Homonuclear ^{13}C 2D correlation spectra were recorded using transfer via dipolar interactions. In particular, proton driven spin diffusion (PDSD, (Bloembergen, 1949)), RFDR (Bennett et al., 1992), and the double-quantum (DQ) recoupling scheme SPC-5 (Hohwy et al., 1999) were employed. A 2D ^{13}C PDSD spectrum was recorded at 500 MHz, using a 800 μs cross polarization (CP)

period, and 10 ms mixing time. Acquisition times were 30 ms in t_2, and 9.5 ms in t_1. The total acquisition time was 67 h. R.f. fields during proton TPPM decoupling and 90° nutation pulses on the observe channel were set to 76 kHz and 63 kHz, respectively. An additional PDSD spectrum was recorded at 600 MHz, using a 1 ms CP period, and 100 ms mixing time. Acquisition times were set to 10 ms and 5 ms in t_2 and t_1, using r.f. ^{1}H decoupling of 94 kHz and ^{13}C fields of 50 kHz, respectively. The total acquisition time was 36 h. The RFDR spectrum was recorded at 500 MHz, using a 1 ms CP and a 1.8 ms mixing time. Acquisition times were 25 ms in t_2, and 9 ms in t_1. The total acquisition time was 41 h. The proton decoupling power was set to 75 kHz using TPPM. The carbon power used was 63 kHz for CP and π/2 pulses, and 25 kHz for the π pulses during the mixing period. Several DQ spectra were recorded at 600 MHz using the SPC-5 sequence (Hohwy et al., 1999) for DQ excitation and reconversion (time: 550 μs). In the DQ spectrum shown below, the carrier frequency was centered in the aliphatic region of the carbon spectrum. Evolution and t_2 detection times were set to 5 ms and 15 ms, respectively, using TPPM decoupling at 80 kHz. The total acquisition time was 15 h. The ^{13}C r.f. field strength during CP was set to 63 kHz and 45 KHz for the π/2 pulses during mixing. J-decoupled PDSD spectra (Straus et al., 1996) were taken at 500 MHz, using mixing times of 30 and 100 ms. The carbonyl selective pulse was a snob pulse, centered at the carbonyl region, of 500 μs length and applied with 5 kHz carbon field strength. Acquisition times were 20 ms in t_2, and 18 ms in t_1. The total acquisition time was 88 h. The proton decoupling power was set to 75 kHz using TPPM. The carbon power used for the CP and hard pulses was 69 kHz.

^{13}C, ^{15}N *heteronuclear spectroscopy.* An NCACB DQ spectrum was taken using a N-Cα selective SPECIFIC-CP (Baldus et al., 1998b) transfer sequence with a mixing time of 2 ms centered at 50 ppm ^{13}C and 105 ppm ^{15}N, employing r.f. field strengths of 15 kHz and 5 kHz for ^{13}C and ^{15}N, respectively. DQ

mixing was achieved using the band-selective HOR-ROR sequence (Nielsen et al., 1994; Verel et al., 1998) for a mixing time of 455 μs. Acquisition times were 15 ms in t_2 and 12 ms in t_1 using TPPM ^{1}H decoupling at 87 kHz in both dimensions. The total acquisition time was 21 h. Two NCOCACB 2D correlation spectra were recorded using different samples and spectral widths. In both cases, SPECIFIC-CP conditions were established during a mixing time of 3 ms with the r.f. carrier frequency centered within the CO region. Subsequently, RFDR (Bennett et al., 1992) mixing (mixing time 1.6 ms) was employed to transfer polarization from CO to Cα resonances. Transfer to side-chain carbons was achieved using PDSD for a mixing time of 10 ms. Acquisition times were 10 ms in the indirect dimension and 8 or 5 ms in the direct dimension. The spectral widths in the indirect dimension were 40 and 110 ppm respectively. The total acquisition times were 71 h for the 8 mg sample, and 25 h for the 20 mg sample. For the ^{1}H-^{15}N CP, transfer times of 1 and 2 ms, respectively, were used.

Processing, assignments and torsion angle calculations

Spectra were processed using the NMRPipe software (Delaglio et al., 1995). Assignments were done using the NMRVIEW program (Johnson and Blevins, 1994). All spectra were referenced to external DSS (Markley et al., 1998). The TALOS (Cornilescu et al., 1999) software was used to predict torsion angles from chemical shifts.

Results and discussion

Solid state NMR sample preparation

A first solid state NMR sample was prepared using the precipitates formed during previous liquid state NMR experiments (Favier et al., 2002). The ^{13}C-^{13}C PDSD spectrum showed broad lines, and collapsed chemical shifts for most of the amino acids, indicating an amorphous state (data not shown). Remarkably, several resonances conserved their liquid state NMR chemical shift. They predominantly correspond to amino acids located within the 4 strand β-sheet, suggesting that at least some residual secondary structure is conserved.

In order to establish conditions for growing crystalline forms of Crh, we carried out an extensive search using home made and commercial (Hampton) crystallization screens. Crystals of different size, quality and stability were obtained under several conditions. Large Crh crystals were obtained using 2 M $(NH_4)_2SO_4$ (shown in Figure 2a) as a crystallization agent resulting in the Crh X-ray structure (Juy et al., 2003). Unfortunately, high salt concentrations are unsuitable for NMR studies. Fine needle crystals were obtained with a wide range of PEG containing screens (PEG 1,000–10,000, 10–30%, pH 6–8), but all of them were unstable over time and/or took several weeks to months to grow. In order to accelerate crystal formation and to stabilize the resulting crystals, the drops were suspended in a closed system over a NaCl reservoir solution. The NaCl concentration was empirically optimized on 4 μl hanging drops in Linbro plates (Hampton) to around 0.2 M NaCl. Since the optimum concentration depends on drop size, up-scaling to 200–400 μl sitting drops required readjustment to around 2 M NaCl. Furthermore, temperature proved to be an important factor. First trials using PEG precipitants over a NaCl solution reservoir at 18 °C yielded very fine precipitates (Figure 2b). Equivalent conditions at 4 °C led to fine needle crystals (Figure 2c). Although protein concentration influences crystal size, slow (one to several weeks) sample precipitation resulted in solid state NMR spectra of excellent quality for all precipitates. It is tempting to hypothesize that the above described protocol should work for other globular proteins as well, as it is well known that proteins generally precipitate in the presence of PEG.

The microcrystals proved to be stable up to temperatures of about 30 degrees (without r.f. irradiation). However, long high power pulse trains simultaneously applied on different channels led to reversible signal loss even at lower temperatures.

Figure 3 shows the resulting 1D ^{13}C CP-MAS spectrum of microcrystalline Crh taken at about 5 °C sample temperature. The spectrum is characterized by the spectral dispersion and line widths of a well-folded, well-ordered protein. While both Ile 47 and 64 Cδ2 and Met 48, 51 Cδ2 are observed at the high field end of the spectrum (vide infra), the Thr 12 Cβ resonance can be detected at the low field end of the aliphatic region (around 74 ppm). The line width of the two Met 48, 51 Cδ resonance amounts to 32 Hz. The remaining lines show some fine structure. The 2D spectra in Figures 4 to 7 discussed below show highly resolved resonance signals suitable for the generation of assignments.
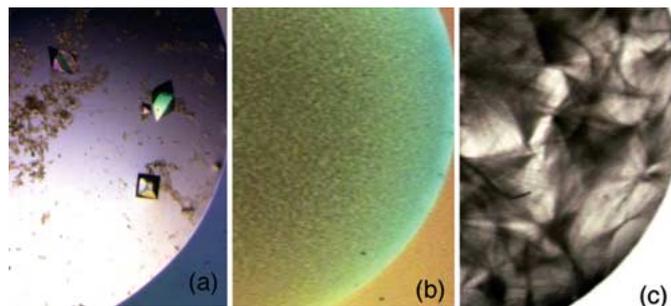
Figure 2. (a) Crh diffracting crystals grown in 2 M $(NH_4)_2SO_4$ used for X-ray crystallography (Juy et al., 2003). (b) PEG precipitate obtained by slow precipitation at 18 °C and (c) PEG precipitate obtained by slow precipitation at 4 °C for the preparation of solid state NMR samples used in the present study. Both precipitates yield the same quality of spectra.
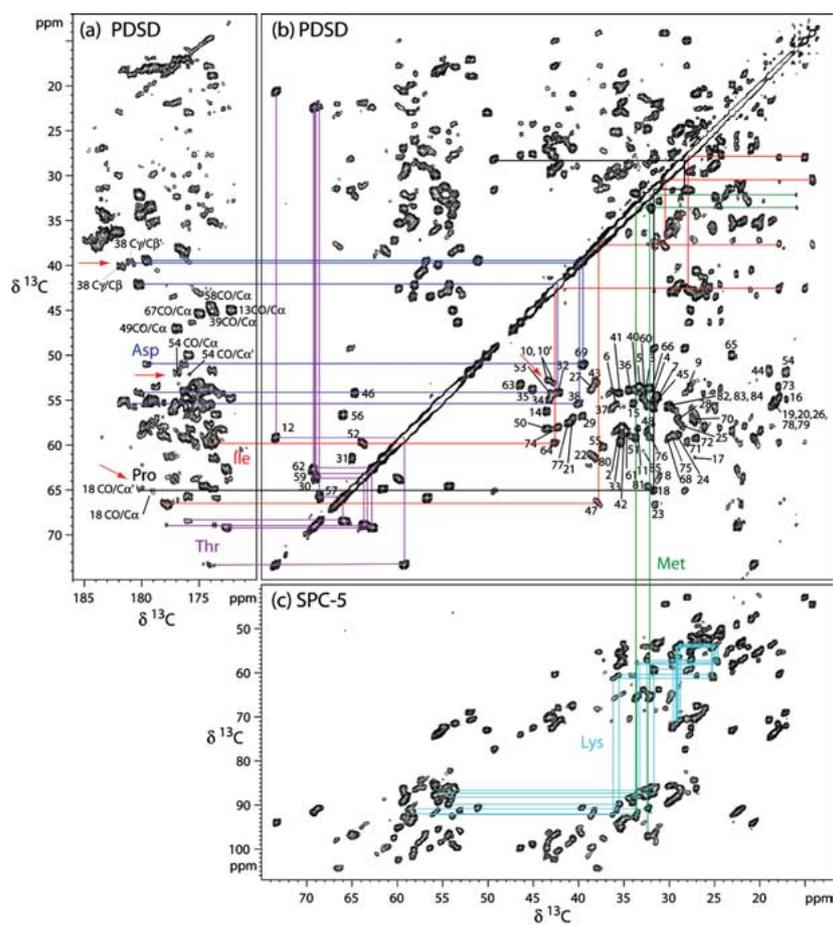

Figure 4. 2D ^{13}C homonuclear correlation spectra of Crh. Spin systems of selected amino acid types are color coded: Asp, violet; Ile, red; Lys, cyan; Met, green; Pro, black; Thr, purple. (a) Carbonyl region of the 2D ^{13}C PDSD correlation spectrum recorded at 500 MHz. The data were processed using linear prediction in the indirect dimension (f1), zero-filling up to 4096 points, a cosine filter and automatic baseline correction in both dimensions. The asterisk indicates the Thr 59 CO/Cα cross peak observed near the noise level. Gly CO/Cα resonance are assigned, and the doubled resonances of Pro 18 CO/Cα, Asp 38 Cδ/Cγ and Ala 54 CO/Cα are indicated by red arrows. (b) Aliphatic region of the 2D ^{13}C PDSD correlation spectrum recorded at 500 MHz. Numbers indicate the Cα/Cβ cross signals of the corresponding amino acid. The pair of Leu 10 Cα/Cβ resonances is highlighted by a red arrow. (c) ^{13}C SPC-5 aliphatic DQ correlation spectrum (recorded at 600 MHz). The data were processed using linear prediction in f1, zero-filling up to 4096 points, a cosine filter and automatic baseline correction in both dimensions.
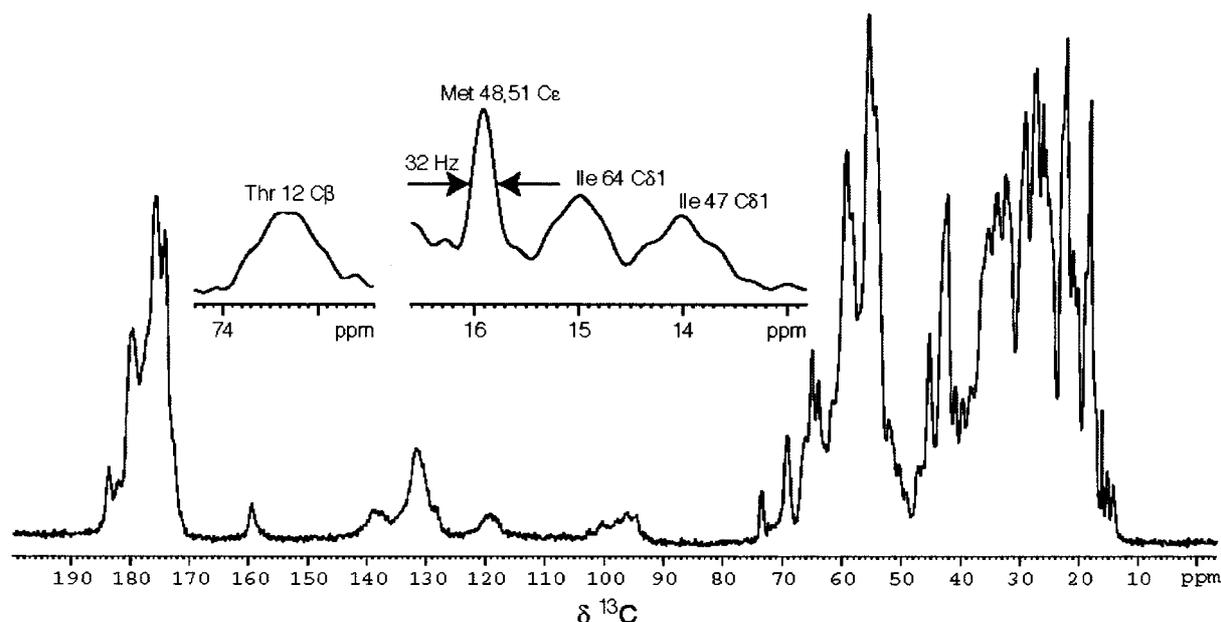
Figure 3. 1D ^{13}C CP-MAS spectrum of PEG precipitated Crh recorded at 500 MHz, 10 kHz spinning speed and 75 kHz proton decoupling using the TPPM decoupling scheme (Bennett et al., 1995). The extracts show the isolated signals from Ile 47, 64 Cδ, Met 48, 51 Cε, and Thr 12 Cβ.

Solid state NMR assignments

As in liquid state NMR, solid state NMR assignments were done using first homo- and heteronuclear spectra correlating spins in the same residue to identify different amino acids and spin systems. For sequential assignments, heteronuclear inter-residue correlations were subsequently established using heteronuclear (^{15}N,^{13}C) polarization transfer experiments.

Intra-residue correlation spectroscopy. Similarly to previous studies involving U-[^{13}C,^{15}N] labeled proteins under MAS conditions (Straus et al., 1998; McDermott et al., 2000; Pauli et al., 2000), intra-residue studies involved, in the first stage, homonuclear (^{13}C,^{13}C) correlation experiments. 2D (1Q,1Q) correlation experiments employing PDSD as a mixing scheme were selected to observe two and three-bond correlations that greatly simplify the identification of amino acid chemical shift systems in the spectrum. In addition, (2Q,1Q) correlation spectra with short 2Q excitation and reconversion times helped to discriminate between one- and multiple-bond correlations. 2Q filtered spectra were also indispensable for the identification of spin systems close to the diagonal of the (1Q,1Q) spectrum. Thus, the combination of both types of (^{13}C,^{13}C) correlation spectra enabled residue

type identification. J-decoupled CO-C(aliphatic) correlation spectra (Straus et al., 1996) were recorded to identify CO resonances and to improve the spectral resolution of the highly abundant Glu and Gln Cδ resonances.

Inter-residue correlation spectroscopy. Combination of homonuclear (^{13}C,^{13}C) correlation experiments with heteronuclear N(i)-Cα(i)-Cβ(i) (NCACB) and N(i)-CO(i-1)-Cα (i-1)-Cβ (i-1) (NCOCACB) experiments allows for sequential assignments by rare-spin correlation spectroscopy (Hong and Griffin, 1998; Hong, 1999; Rienstra et al., 2000; Pauli et al., 2001; Detken et al., 2001; Jaroniec et al., 2002; Petkova et al., 2003). Similar to previous studies (Pauli et al., 2001; Jaroniec et al., 2002; Petkova et al., 2003), frequency selective N-C polarization transfer was established using SPECIFIC-CP conditions (Baldus et al., 1998b). Likewise, CA-CB polarization transfer involved zero-quantum (0Q) PDSD or double-quantum (2Q) transfer. For polarization transfer originating from non-protonated CO to aliphatic carbons within NCOCA-type experiments, we implemented the RFDR (Bennett et al., 1992) mixing scheme. As previously demonstrated (Bennett et al., 1992; Baldus et al., 1998a), RFDR mixing is particularly well suited for band-selective polarization transfer around

$\Delta\Omega \sim n\omega_R$ (n = 1,2) where $\Delta\Omega$ represents the isotopic chemical shift difference in the spin pair of interest and ω_R the MAS rate. RFDR-based CO-CA polarization transfer is hence most effective for typical CO-CA chemical differences at magnetic fields at or above 500 MHz for medium to high MAS rates. Additional attempts to replace the subsequent ^{13}C-^{13}C spin diffusion step by double-quantum (r.f. driven) polarization transfer failed as it resulted in sample heating and signal loss by excess of r.f. irradiation.

Amino acid spin system identification. Previously determined NMR solution state chemical shifts of the Crh monomer were not used at any stage of the spectral assignment procedure. In fact, important differences were identified already at an early stage by comparison between a simulated ^{13}C-^{13}C correlation spectrum using the liquid state chemical shifts, and the PDSD solid state NMR spectrum. This already insinuated a different form of Crh in the microcrystalline solid state sample, obviously proscribing direct chemical shift inference. Instead, intra-residue (^{13}C,^{13}C) spin systems were identified following a similar procedure to the one well established for liquid state NMR (Wüthrich, 1986), using the characteristic signal patterns, as well as the typical chemical shifts as reported in the BMRB (Seavey et al., 1991).

Figures 4a and b show extracts of the 2D ^{13}C-^{13}C PDSD spectrum recorded with 10 ms mixing time at 500 MHz. The spectrum predominantly shows one and two bond connectivities, but for several amino acids 3 bond transfers are also present. Most spin systems could be identified using this spectrum. Examples involving Asp, Ile, Lys, Met, Pro and Thr are indicated in Figures 4a–c. Cα-Cβ cross peak assignments are indicated in the aliphatic part (Figure 4b). For the glycines, CO-Cα assignments are indicated in Figure 4a. The aliphatic part of the seven Lys spin systems is highlighted in the extract of the DQ-SPC-5 2D spectrum in Figure 4c. This spectrum proved to be essential for differentiation between one bond and multiple-bond transfers.

A further spectral analysis depends on the type of amino acid under study. Most alanines (Ala 16, 19, 20, 26, 44, 54, 65, 73, 78, 79), leucines (Leu 10, 14, 21, 35, 50, 63, 72, 74, 77), valines (Val 2, 6, 8, 23, 33, 42, 55, 61, 81, 85), and isoleucines (Ile 47, 64) were readily identified by the typical chemical shift patterns, and multiple-bond cross signals involving their methyl group(s) in isolated regions of the spectrum. Glycine (Gly 13, 39, 49, 58, 67) reson-

ances were identified by their isolated CO-Cα cross signals in the carbonyl region. Resonances relating to the only proline residue (Pro 18) were easily observed due to the characteristic chemical shift pattern. The aromatic residues phenylalanine (Phe 22, 29, 34) and tyrosine (Tyr 80) could be identified due to their low abundance and the typical chemical shift of their Cα-Cγ and Cβ-Cγ cross signals. Cross peak signals between aromatic carbons showed weak intensity and were partly obscured by aromatic resonances from the non-ordered 6xHis tag residues (data not shown). The characteristic Cβ chemical shifts at the downfield limit of the aliphatic spectrum allowed for a straightforward identification of the four serine (Ser 31, 46, 52, 56) and five threonine (Thr 12, 30, 57, 59, 62) residues in the spectrum. The degeneracy between the two threonine residues (Thr 30, 59) could be removed by investigation of correlations involving CO resonances.

The long side chains of arginine and lysine made the spectral distinction among their CH$_2$ resonances problematic. Many of the lysine residues (Lys 5, 11, 37, 40, 41, 45, 76) were tentatively identified in a first step, and either confirmed or corrected by sequential assignments. Two of the three arginine residues (Arg 9, 17, 28) could only be spotted after sequential assignment (Arg 9, 17). Arg Nε/Cζ cross signals could be observed in the NCOCACB spectra, but could not be assigned to their corresponding amino acids. Aspartic acid (Asp 32, 38, 69) and asparagine (Asn 27, 43) resonances were easily identified using the Cγ-Cβ and Cγ-Cα cross signals observed in the RFDR and PDSD spectra.

Glutamine (Gln 3, 4, 15, 24, 66, 71, 82) and glutamic acid (Glu 7, 25, 36, 60, 68, 70, 72, 83, 84) can in principle be identified in a similar manner starting at their Cδ chemical shifts. However, they are very abundant in Crh, and the Cδ shifts show only a poor dispersion, making identification difficult. In order to maximize spectral resolution between Glu Cδ-(Cγ,Cβ,Cα) cross signals, we used J-decoupled carbonyl – C(aliphatic) 2D correlation spectroscopy (Straus et al., 1996) with different mixing times (Figure 5a). The Glu Cδ chemical shifts are isolated at the low field end of the spectrum around 183 ppm. Given the high spectral resolution provided by J-decoupling in the indirect dimension, correlation patterns for all ten Glu residues can be established. Figure 5 shows the spin systems of the ten Glu residues, starting at the Cδ/Cα cross signals in the J-decoupled PDSD spectrum in Figure 5a, and down to their Cα/Cβ cross signals in the DQ-SPC5 spectrum in Figure 5b. It is
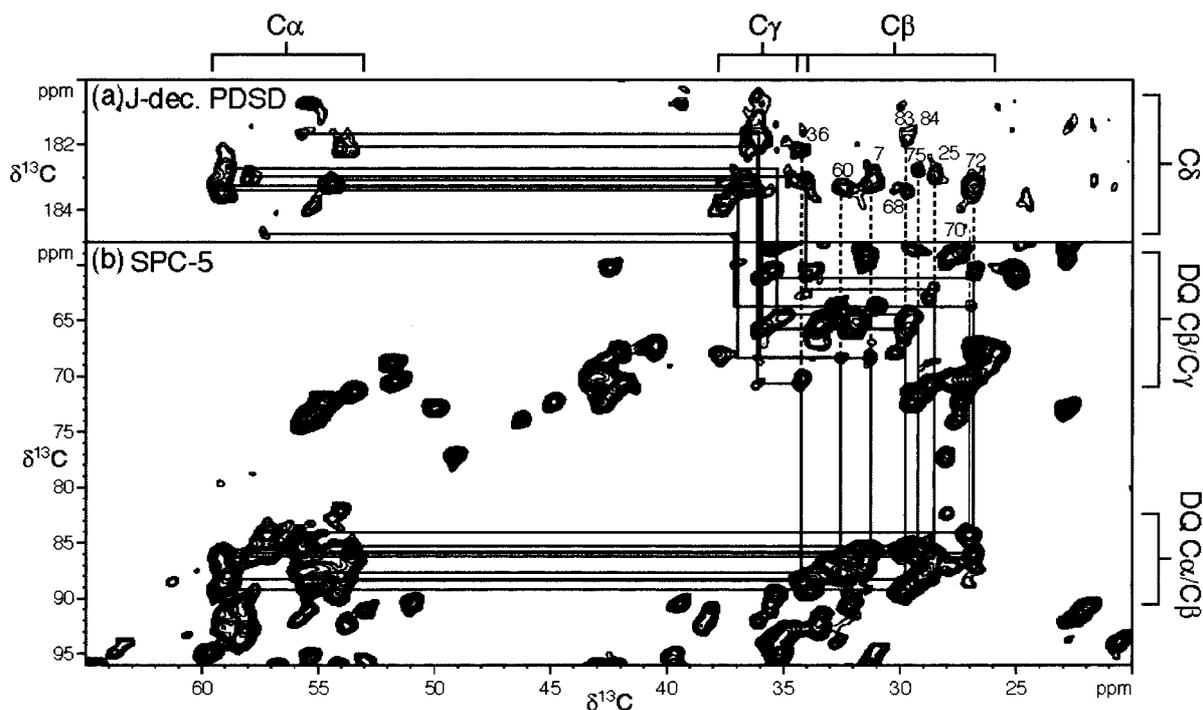
Figure 5. Assignments of Glu residues. (a) Extract of the J-decoupled PDSD spectrum recorded at 500 MHz using 100 ms mixing time showing the Glu Cδ/Cα,Cβ,Cγ cross signals. The data were processed using zero filling, cosine filter and automatic baseline correction in both dimensions. (b) Extract of the ^{13}C SPC-5 aliphatic DQ correlation spectrum recorded at 600 MHz. The data were processed as indicated in the legend of Figure 4c. The spin systems of the ten Glu residues of Crh are indicated by solid lines starting from Cδ in f1 in the upper spectrum (Figure 5a), to the Cα chemical shift in f2 in the lower spectrum (Figure 5b), via Cγ and Cβ resonances. Dashed lines correlate the spin systems to the Cδ/Cβ cross signals observed in the J-decoupled spectrum.

clear that the best resolved signals are the Cδ-Cβ cross peaks in the J-decoupled spectrum, underlining the importance of the strategy used.

The Gln Cδ chemical shifts are observed more up-field (around 180 ppm, Figure 4a) and less isolated due to spectral overlap with backbone CO signals. The RFDR spectrum was used to identify the Gln Cδ-Cγ resonances, since only one-bond correlations were found in this spectrum at short mixing times (data not shown). One Glutamine (Gln 3) was found to have an outlier ^{15}N chemical shift, at 82.6 ppm (Figure 6a). Indeed, careful analysis of the homo- and heteronuclear spectra shows that the observed spin system is a Cα-Cβ-Cγ spin system in the aliphatic region. In the NCACB DQ spectrum, a positive-negative-positive pattern (Baldus, 2002) is observed (Figure 6a) with chemical shift values typical for Cα, Cβ and Cγ. The same spin system is observed in the PDSD spectrum with 10 ms mixing time, correlated to a CO carbon at 172.2 ppm (Figure 6b). The peak intensities decrease with decreasing ppm values, confirming that the resonance at 54.9 ppm is indeed the Cα, the Cβ at 32.7 ppm,

and the Cγ at 30.9 ppm. In the PDSD spectrum with 100 ms mixing time (Figure 6c), no additional cross peaks were observed, excluding the possibility of a larger spin system. In line with expectations, the CO-Cα correlation is exclusively observed in the RFDR spectrum (Figure 6d).

The Asn 27, 43 side chain Nδ2 chemical shifts could be identified in the NCOCACB spectrum by their Nδ2 /Cα, Cβ cross signals. Gln Nε2 resonances were equally observed in these spectra, but showed too much overlap for assignment.

Due to spectral overlap between Cβ and Cγ shifts, the three methionine (Met 1, 48, 51) residues must be analyzed as a virtual 2-spin system. Two Cγ-Cε cross signals were readily observed in the PDSD spectrum (Figure 4b). Weak cross peaks at the corresponding Cγ frequency were observed close to the diagonal in the 2Q spectrum (Figure 4c), leading to identification of Met 48 and 51. Met 1 seems to escape detection, which would be consistent with partial processing of Met 1 during Crh expression in *E. coli* (Favier et al., 2002).
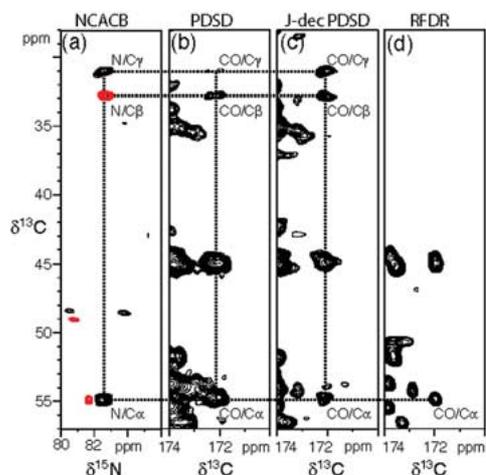
Figure 6. Extracts from different spectra showing the Gln 3 spin system. (a) Extract of the NCACB DQ correlation spectrum (for processing parameters, see legend of Figure 7a). (b) Extract of the PDSD spectrum with a 10 ms mixing time (processing as described in legend of Figure 4a). (c) Extract from the J-decoupled PDSD spectrum with a 100 ms mixing time (processing as described in legend of Figure 5a). (d) Extract of the RFDR spectrum with 1.8 ms mixing time, processed with zero-filling up to 4096 points, cosine filter, and automatic base-line correction
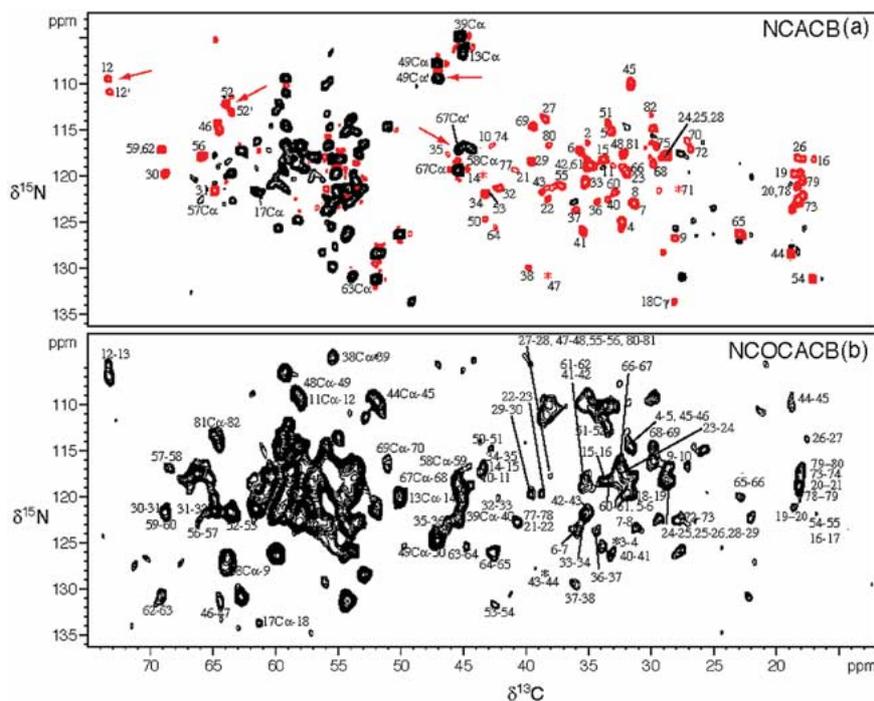

Figure 7. (a) NCACB DQ correlation spectrum recorded at 600 MHz. The data were processed with linear prediction up to 240 points in f1, zero filling to 4096 points, cosine filters and automatic baseline correction in both dimensions. Positive peaks (black) correspond to ^{15}N-^{13}C one- and three-bond correlations, and negative (red) to two-bond correlations. Amino acid assignments are shown for the N-Cβ cross signals. When this was not possible, N-Cα or Cγ correlations are indicated instead. Red arrows point to doubled resonance signals. (b) NCOCACB correlation spectrum recorded at 600 MHz. The data are processed with linear prediction up to 160 points in f1, zero filling to 4096 points, cosine filters and automatic baseline correction in both dimensions. Sequential assignments for N(i)-Cβ(i-1) correlations are indicated on the spectrum. For some amino acids, only the Ni-Cα(i-1) could be observed. Positions marked with an asterisk indicate either signals close to the noise or signals only observed in another NCOCACB correlation spectrum (data not shown).

Due to the very high quality of the NCACB DQ correlation spectrum (Figure 7a), identification of the ^{15}N shifts was mostly straightforward by comparison with the corresponding Cα and Cβ shifts in the 2D ^{13}C PDSD (Figure 4b) or DQ (Figure 4c) correlation spectrum. Notably, a few peaks could not be observed in the NCACB DQ spectrum, but were present in the NCACB PDSD spectrum (not shown). For some of these correlations, peak cancellation occurs in the regions where both positive and negative signals (partially) overlap in the spectrum. Figure 7a shows the assignments for N-Cβ cross signals. Signals close to the noise level or only observed in the NCACB PDSD are marked with an asterisk. For residues where N-Cβ cross signals are not observed, N-Cα correlations are indicated instead. For several Thr, Leu (such as Leu 63) and Ile residues, N-Cγ correlation can be observed indicative of a two-bond transfer for the given 2Q mixing time.

Even if not complete, identification of amino acid spin systems is essential for sequential assignments of a protein of the considered size. In particular, knowledge of the possible amino acid specific resonance sets allowed us to resolve ambiguities in the sequential assignment procedure discussed below.

Sequential assignment. Each protein sequence presents several potential starting points for sequential assignments. These are generally pairs of residues with typical chemical shifts, or residues that are easy to identify due to their low abundance in the sequence. An unequivocal assignment solution can be found for several pairs. For others, the number of possible solutions can be reduced by continuing the assignment towards the N-or C-terminus.

Figure 7b shows one of the NCOCACB spectra used for sequential assignments. At a given ^{15}N shift of amino acid i identified in the NCACB spectrum, the Cα-Cβ pair of amino acid i-1 was searched in the NCOCACB spectrum. Sequential assignments were predominantly obtained from a spectral analysis of the aliphatic region of the spectra. The carbonyl region proved useful for residues with isolated ^{15}N chemical shifts, such as glycine or proline. Figure 7b shows the assignments for the N-Cβ cross signals. Signals close to noise level or only observed in the other NCACB spectra are marked with an asterisk. For residues where no N-Cβ cross peak was observed, N-Cα cross signals are indicated instead. For example, Arg 17 shows very weak cross signals, and no side chain assignment could be obtained beyond Cβ. In the

NCACB spectrum, only the N-Cβ cross peak is present at δ^{15}N 121.4 ppm / δ^{13}Cα 61.4 ppm (Figure 7a). Arg 17 could only be assigned by its N(i+1)-Cα(i) correlation present in the NCOCACB spectrum at δ^{15}N 133.3 ppm / δ^{13}Cα 61.4 ppm (Figure 7b), the unequivocal identification of the (i+1) nitrogen shift belonging to proline 18 as the unique proline in the sequence. In addition, the prior assignment of Thr 30 and Tyr 80, which show similar Cα chemical shifts to Arg 17 was compulsory. Weak cross signals for Arg 17 have also been observed in the liquid state spectra, and have been attributed to conformational exchange in this region (Favier et al., 2002).

It should be noted that for a restricted set of residues, two chemical shifts were observed for the same spin (red arrows in Figures 4a,b and 7a). This will be discussed in more detail below.

To summarize, Table 1 lists the solid state chemical shift assignments obtained for the microcrystalline form of Crh. Assignments were successful for 99% of N, Cα, and Cβ atoms, 67% of Co, and 87% of the side chain carbon, resulting in a total of 88%.

Structural analysis

Comparison with monomer liquid state NMR chemical shifts. In Figure 8, we present a comparison between the N, Cα and Cβ monomer liquid state NMR resonance assignments and the solid state chemical shifts. Note that no liquid state chemical shifts were reported for residues 1-3 (Favier et al., 2002). [15]N chemical shifts show in general larger deviations with a mean value of 2 ppm (Figure 8a) compared to an average of 1 ppm for ^{13}C chemical shifts (Figures 8b,c), which might be partly due to the difference of the pH between the liquid state and solid state samples.

The largest chemical shift differences between liquid state and solid state NMR resonance assignments are observed in three regions of the protein. This is illustrated in Figures 8d and 8e, where the sum of the absolute values of the chemical shift differences from N, Cα and Cβ are color coded on the Crh dimer (Figure 8d, PDB code 1mu4 (Juy et al., 2003)) and on the monomer (PDB code 1k1c (Favier et al., 2002)) structures. Deep blue corresponds to the smallest differences, red to the largest differences, as indicated on the scale.

The large chemical shift differences between solution and solid state NMR can be attributed to the dimerization state of Crh, as illustrated in Figures 8d,e. Indeed, in a single crystalline state, Crh undergoes

Table 1. Solid state chemical shift table of the Crh dimer. These chemical shifts have been deposited with the BioMagResBank (BMRB) under the accession number 5757

Res.	^{15}N	^{13}CO	^{13}C$^\alpha$	^{13}C$^\beta$	^{13}C$^\gamma$	^{13}C$^\delta$	^{13}C$^\varepsilon$	^{13}C$^\zeta$	^{15}N$^\delta$
M1									
V2	116.5	174.0	58.0	35.1	21.5/21.5				
Q3	82.6	172.2	54.9	32.7	30.9				
Q4	125.2	174.1	55.5	32.2	33.2	180.2			
K5	115.2	174.9	53.5	33.2	24.5	28.8	40.1		
V6	117.4	175.6	55.5	35.6	22.9/19.8				
E7	123.3	175.4	54.5	31.3	36.8	182.9			
V8	122.7	176.8	63.7	31.1	22.4/21.6				
R9	126.8		54.1	28.0					
L10	116.7		52.9	43.0	25.5	21.0/21.0			
			53.1^a	43.6^a					
K11	118.6	174.1	58.1	33.3					
T12	109.5	173.8	59.1	73.4	20.7				
	111.0^a								
G13	106.4	172.1	44.9						
L14	120.0	177.2	56.2	43.4	26.6	24.8/24.8			
Q15	118.4	174.1	55.3	33.8	32.1	180.1			
A16	118.2	179.1	54.9	16.9					
R17	121.4	177.5	61.4	27.2					
P18	133.6	180.0	65.1	31.6	28.2	49.2			
		178.8^a							
A19	119.8		55.5	18.3					
A20	121.5		54.8	18.3					
L21	119.6	178.6	56.9	40.6	26.9	20.8/20.8			
F22	122.6	177.6	61.1	38.4	138.9	131.6/131.6			
V23	120.2	177.0	66.6	31.5	23.3/22.0				
Q24	118.3		58.7	29.0	34.2	180.1			
E25	117.9		57.8	28.6	34.4	182.7			
A26	118.2		54.6	17.8					
N27	113.9		53.8	38.4	176.1				110.3
R28	117.9		57.2	28.9	27.4	42.8			
F29	118.5	175.8	56.8	39.6	140.5	131.5/131.5			
T30	119.8	177.7	63.8	68.7	21.9				
S31	121.6	173.7	61.6	64.9					
D32	121.5	175.5	54.2	42.2	180.2				
V33	120.8	173.9	59.6	35.2	20.0/22.2				
F34	122.0	174.9	55.0	43.1	138.7	131.6/131.6			
L35	117.7	175.6	53.2	46.3	27.6	25.4/24.2			
E36	122.9	174.7	53.8	34.3	36.3	182.0			
K37	123.8		55.8	36.1	25.0	28.9	42.1		
D38	129.9	175.5	55.4	39.6	180.9				
				40^a	181.7^a				
G39	105.0	173.8	45.0						
K40	122.6		54.0	33.5	25.0	28.9	42.1		
K41	126.0		54.1	35.4	25.2	28.9	40.7		

V42	118.8		57.9	35.0	21.6/18.4			
N43	121.4	174.9	53.0	38.1	176.7			111.0
A44	128.4	173.8	51.8	18.9				
K45	110.2	175.5	55.6	31.5	27.4	29.5	42.8	
S46	114.9	174.4	54.2	64.6				
I47	131.0	178.0	66.4	37.7	30.4/17.8	14.1		
M48	117.7		58.3	32.3	32.2		15.9	
G49	107.9	176.9	46.9					
	109.5a							
L50	124.8	179.7	58.2	43.3				
M51	114.3		59.1	33.6	33.5		15.8	
S52	112.3	175.2	59.8	63.8				
	113.1a							
L53	122.0		54.2	42.8	26.1	22.4/22.4		
A54	131.2	176.8	51.8	17.1				
		175.7a						
V55	121.2	180.9	60.2	37.1	22.9/20.0			
S56	118.0	173.5	56.7	65.9				
T57	122.4	175.8	65.8	68.4	22.4			
G58	117.1	173.9	44.4					
T59	117.2	172.4	63.0	68.8	22.4			
E60	121.8		54.3	32.7	36.3	183.2		
V61	118.9		58.4	34.8	19.8/22.9			
T62	117.2	172.6	62.6	69.1	22.5			
L63	131.0		53.8	45.0	27.6	24.2/24.2		
I64	125.8	173.9	59.8	42.6	28.0/17.8	15.0		
A65	126.4	175.9	50.0	23.0				
Q66	120.1	174.2	53.7	32.1	33.4	179.1		
G67	119.5	174.9	45.2					
	117.1a							
E68	118.7		59.2	29.9	36.2	183.3		
D69	114.8	176.2	51.1	39.4	179.6			
E70	116.3	175.1	57.4	27.2	36.9	184.5		
Q71	121.4		59.5	27.7	33.8	179.7		
E72	117.1		59.3	26.8	34.2	183.2		
A73	122.7	178.7	53.5	17.9				
L74	116.5		58.0	42.1	26.0	24.3/24.3		
E75	116.9	176.2	58.9	29.4	36.2	182.6		
K76	118.9		59.0	32.2	24.8	28.6	42.1	
L77	119.4	179.1	57.5	40.9	26.8	22.5/22.5		
A78	121.1	181.5	55.1	18.2				
A79	120.1	180.9	55.6	18.7				
Y80	116.8	176.8	61.3	38.0	129.7	132.8/132.8	118.2/118.2	157.3
V81	117.8	174.6	64.6	32.2	23.5/22.1			
Q82	113.4		55.7	29.9	35.1	179.0		
E83	114.9		55.7	30.0	36.2	181.7		
E84	114.9		55.3	29.8	36.2	181.7		
V85	93.4	171.1	60.6	32.7	21.3/19.3			

aDoubled resonances.

conformational changes upon dimerization in several regions of the monomer structure (Juy et al., 2003). The most drastic conformational differences are observed in the hinge region and comprise residues Lys 11- Gln 15, which cross the dimer interface and connect the core of each chain to its corresponding swapped β1-strand. In the NMR-derived structure of the monomer, this segment forms loop 1, which is folded onto the hydrophobic core of the protein to create a flat surface. Domain swapping also induces β-strand 1 to shift by two residues on Crh dimerization, to complete the 4 strand β-sheet with β-strands 2-4 from the other monomer, but with different hydrogen bonding partners (Juy et al., 2003). Furthermore, conformational rearrangements upon dimerization are observed for helix B where several residues undergo significant displacements. Helix B is extended in the dimeric form and comprises residues Ser 46-Ser 52, as opposed to Ile 47-Leu 50 in the monomer. Residues Met 51-Thr 59 in the monomer form loop 2 (Leu 53-Thr 59 in the dimer). This loop stabilizes loop 1 in the monomer, while it is located at the dimer interface in the crystal structure (Juy et al., 2003).

With these conformational changes in mind, the observed chemical shift differences become clear. The first group of residues with very different chemical shifts is located at the N terminus around residues Gln 4-Arg 17, corresponding to β1-strand and loop 1 in the Crh monomer (illustrated in Figures 8d,e). As a result of the conformational changes described above, β-strand 1 hydrogen bonding partners are different for residues Val 2-Arg 9 in the dimer, and Val 8 and Arg 9 form no longer part of the β∥-strand. Hydrogen bonding patterns and torsion angles of residues Leu 10-Leu 14 forming the β1a-sheet in the hinge region of the dimer are altogether different in the monomer.

The second region with large chemical shift differences comprises residues Ile 47-Glu 60. Residues Ile 47-Leu 50 form helix B in the monomer, experiencing important conformational changes upon dimerization as described above. Loop 2 forms hydrogen bonds with loop 1 in the monomer, while it is located at the dimer interface in the crystal structure. For example, Thr 57 forms an intermolecular hydrogen bond with Thr 12 in the dimer, whereas Thr 12 is hydrogen bonded to Ala 54 in the monomer. The third region is located near the C terminus, and its conformation strongly differs between the monomer and dimer. Probably, crystal contacts determine the conformation

of the C-terminus including the LQ(6×His) extension, whereas this part of the protein is flexible in solution.

In summary, the observation of the dimeric form thus seems a good rationale for the observed chemical shift differences. This is also illustrated in the following paragraph where the solid state NMR chemical shifts are used to predict the corresponding dihedral angles.

Dihedral angle predictions. The chemical shift assignments obtained on microcrystalline Crh can be used to define conformation dependent chemical shifts. Employing the TALOS program (Cornilescu et al., 1999) these parameters have been exploited to predict dihedral angles from the assigned N, CO, Cα and Cβ solid state NMR chemical shifts. Figure 9a shows the differences between the predicted ψ angles and those of the Crh monomer structure. Most angles differ by less than 40 degrees, with a mean value of 34 degrees. Notably, three regions can be identified where significantly larger deviations are observed. These include residues Arg 9-Gln 15, Leu 53-Val 55, and Gly 67-Glu 70. The corresponding residues are indicated in red on the monomer structure in Figure 9c. Two of these regions (Arg 9-Gln 15, Leu 53-Val 55) overlap with those already identified by the variations in chemical shifts between liquid state and solid state NMR data. As described in the preceding paragraph, these regions experience the most pronounced conformational changes during the monomer to dimer transition. Thr 30 and Gly 67-Glu 70 are located in loops pointing to the outside of the protein, and could possibly show different conformations induced by crystal contacts in the dimer.

In Figure 9b, we present a comparison between the dihedral angles calculated from the solid state NMR chemical shifts with the ones observed for the domain swapped dimeric structure determined by X-ray crystallography (Figure 9d). Only Thr 30 and Gln 83,84 show large differences and are highlighted in red on the dimer structure in Figure 9d. Conformational differences within these residues could be explained by variations in crystal contacts between the microcrystalline and single-crystal form of Crh prepared under different experimental conditions. Taken together, these data suggest that Crh almost certainly exists as a dimer in the microcrystals.

Doubled resonance signals. Remarkably, several residues are characterized by doubled NMR resonance signals (indicated by arrows in Figures 4a,b and 7a).

Figure 8. Chemical shift differences between the liquid state NMR Crh monomer and solid state NMR Crh dimer. Secondary structures of the monomeric and dimeric form are shown below the graphs. (a) ^{15}N backbone, (b) ^{13}Cα, (c) ^{13}Cβ chemical shift differences for Crh residues 3–84 (no liquid state assignments are available for residues 1–3 (Favier et al., 2002)). (d) Sum of the absolute values of ^{15}N backbone, ^{13}Cα, and ^{13}Cβ chemical shift differences color coded on the Crh dimer crystal structure (PDB code 1mu4 (Juy et al., 2003)) and (e) on the Crh monomer structure (PDB code 1k1c (Favier et al., 2002)). Colors vary from blue for smallest chemical shift differences, to red for largest deviations, corresponding chemical shift differences are indicated. Black stands for not applicable. All structures were drawn using Swiss-PDBViewer (Guex and Peitsch, 1997) and rendered with POV-Ray^{TM}.

Figure 9. Comparison between the dihedral ψ angles predicted from the solid state NMR chemical shifts using the TALOS (Cornilescu et al., 1999) software and those of the monomer and dimer Crh structure. (a) Absolute values $|\Delta(\psi_{monomer} - \psi_{TALOS})|$ plotted as a function of residue number. Residues showing large deviations are highlighted in red. The secondary structure of the Crh monomer is shown above the graph. (b) Absolute values $|\Delta(\psi_{dimer} - \psi_{TALOS})|$ plotted as a function of residue number. Residues with large deviations are highlighted in red. The secondary structure of the Crh dimer is shown above the graph. (c) Location of highlighted amino acids on the monomer structure (PDB code 1k1c (Favier et al., 2002) and (d) on the dimer structure (PDB code 1mu4 (Juy et al., 2003)).

Two sets of nitrogen chemical shifts were detected for Thr 12, Gly 49, Ser 52 and Gly 67 (Figure 7a). In addition, ^{13}C signal pairs were identified for the Cα, Cβ shifts of Leu 10 , the CO of Pro 18 and Ala 54 and the Cδ, Cγ of Asp 38 (Figures 4a,b, indicated by red arrows). It is striking that all but two of the residues showing NMR signal pairs are located at the dimer interface or near helix B (residues Leu 10, Thr 12, Pro 18, Gly 49, Ser 52 and Ala 54, color coded in red in Figure 10, referred to as group one). Asp 38 and Gly 67 form the second group and are found in loops exposed on the surface of the protein (labeled in green in Figure 10).

There are at least three different possible rationales for these spectroscopic observations. First, the two signals could reflect conformational differences between the two monomers in the dimer. This is however not very likely, since in the dimer structure determined by X-ray crystallography (Juy et al., 2003), only minor differences exist between the conformations of the two monomers, with average differences between φ and ψ dihedral angles smaller than 5°, and an overall r.m.s. deviation of 0.7 Å for backbone atoms. A second possibility is that the two signals have their origin in different conformations of the Crh dimers in the crystallographic unit cell caused by different crystal contacts. A third explanation could involve dynamic behavior, for instance slow exchange between two conformational states.

In the first group of residues located at the dimer interface and the nearby helix B, all concerned atoms belong to the backbone or to buried side chains. For these residues, different crystal contacts seem to be a less convincing explanation. In contrast, an increased flexibility of the Crh polypeptide chain in this region might be important for binding of Crh to its biological partners, as Helix B and loop 2 should be key positions as to the interaction between Crh with

CcpA (Jones et al., 1997) or HprK/P (Fieulaine et al., 2002). Furthermore, flexibility might even play a major role in the domain swapping mechanism, which particularly affects this region (Juy et al., 2003). For the second group of doubled resonances including Asp 38 and Gly 67, both different crystal contacts, as well as increased loop dynamics, could be plausible explications.

Notably, increased flexibility has been identified in the Crh monomer liquid state NMR study for the turn connecting the β-strands 2 and 3 (including Asp 38), as well as for helix B (residues Met 48-Ala 54) (Favier et al., 2002). The time scale of these dynamic processes was shown to include contributions on the nanosecond timescale, as well as on the millisecond timescale. The authors concluded that the increased flexibility of the Crh polypeptide chain observed near the regulatory site may be important for binding in the active site of HprK/P and/or the interaction with CcpA. However, further experimental investigations are needed in order to confirm the static or dynamic nature of the observed peak doubling in the dimeric form of Crh.

Conclusions

We have developed a protocol for solid state NMR sample preparation and demonstrated that an optimized set of homo– and heteronuclear correlation experiments can lead to nearly complete spectral assignments of a 10 kDa, solid-phase protein at medium-size magnetic fields. Our study confirms that ssNMR studies using uniformly labeled protein variants permit a detailed analysis of the backbone conformation of the protein of interest. In the current context, backbone dihedral predictions can be derived from chemical shifts that allow for a direct structural comparison of
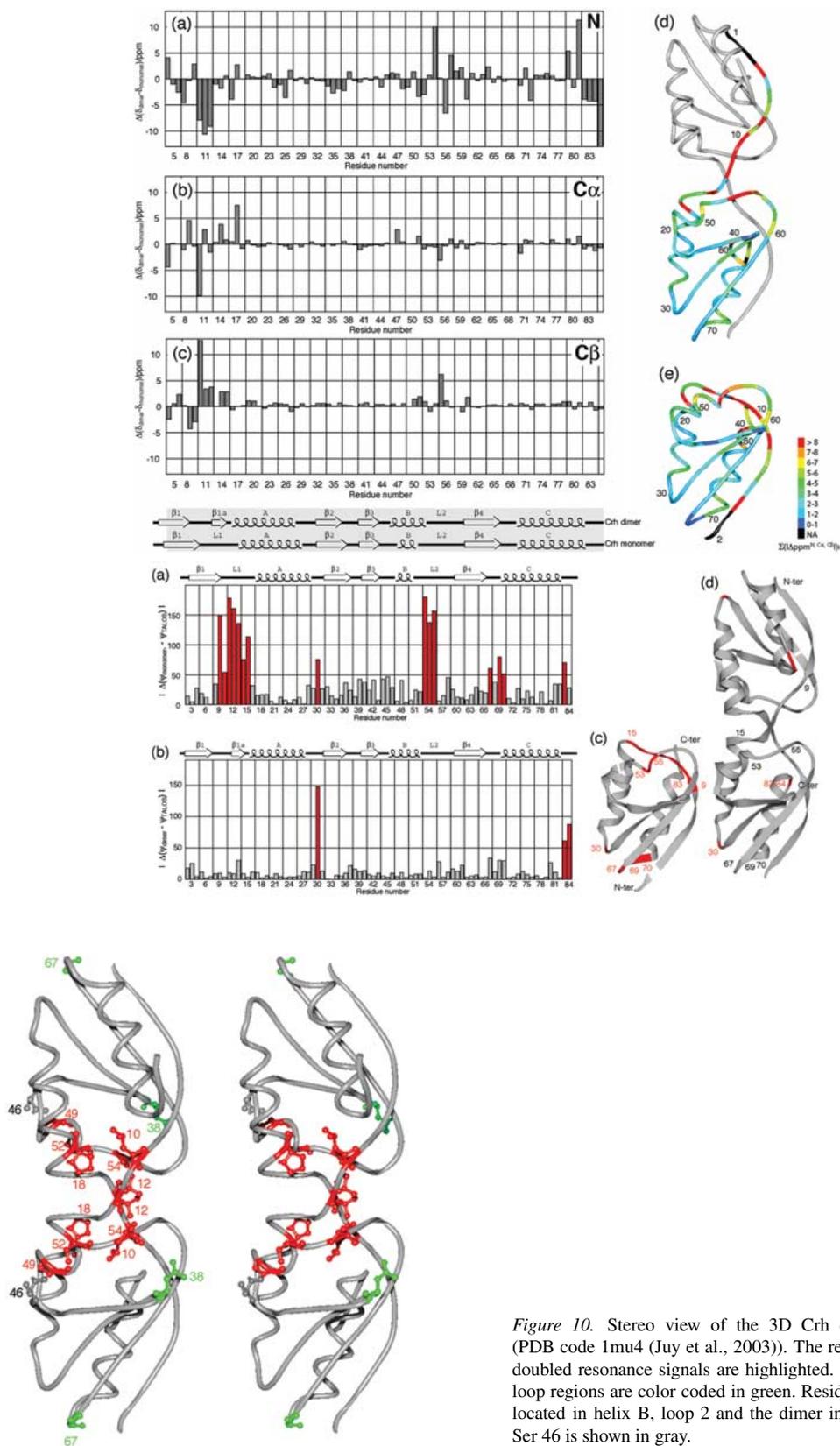
Figure 10. Stereo view of the 3D Crh dimer crystal structure (PDB code 1mu4 (Juy et al., 2003)). The residues characterized by doubled resonance signals are highlighted. Residues located in the loop regions are color coded in green. Residues indicated in red are located in helix B, loop 2 and the dimer interface. The active site Ser 46 is shown in gray.

338

the solid state sample to isoforms of the protein in other chemical environments. Our data strongly indicate that the microcrystalline Crh sample adopts a conformation that is highly similar to the 3D domain swapped dimeric Crh structure observed in a single crystal study. Chemical shift changes discriminating the monomeric from the dimeric structure of Crh have been readily identified. Doubled resonance signals of several strategic residues might indicate dynamics present in the protein and could potentially be important for understanding the interactions between Crh and its partners, and/or the domain swapping mechanism.

The presented data provide a solid basis for further structural investigations of Crh and its interaction partners. For instance, solid-state NMR chemical shift mapping should already supply an answer as to the multimerization state of P-Ser-Crh in interaction with CcpA. In addition, our data, together with NMR data obtained in the solution state, may serve as a valuable reference to investigate disordered states, as observed in the spontaneously formed precipitate mentioned above. Investigation of other disordered states might help to elucidate the conformational transition of a solution state monomer to a crystalline domain swapped dimer. Moreover, Crh may serve as a valuable model system for additional solid state NMR technique developments, for example in the context of studying protein structure, dynamics or protein-protein interactions. Solid-state NMR studies as outlined here may hence provide a complementary means to investigate multimerization processes and other protein-protein interactions at atomic resolution. In particular, they may form the basis for structural investigations of large protein-protein complexes that are difficult to study by solution state methods.

References

Andrew, E.R., Bradbury, A. and Eades, R.G. (1958) *Nature*, **4650**, 1659.

Baldus, M. (2002) *Prog. Nucl. Magn. Reson. Spectrosc.*, **41**, 1–47.

Baldus, M., Geurts, D.G. and Meier, B.H. (1998a) *Solid State Nucl. Magn. Reson.*, **11**, 157–168.

Baldus, M., Petkova, A.T., Herzfeld, J. and Griffin, R.G. (1998b) *Mol. Phys.*, **95**, 1197–1207.

Bennett, A.E., Ok, J.H., Griffin, R.G. and Vega, S. (1992) *J. Chem. Phys.*, **96**, 8624–8627.

Bennett, A.E., Rienstra, C.M., Auger, M., Lakshmi, K.V. and Griffin, R.G. (1995) *J. Chem. Phys.*, **103**, 6951–6958.

Bloembergen, N. (1949) *Physica*, **15**, 386–426.

Böckmann, A. and McDermott, A.E. (2002) In *The Encyclopedia of NMR*, Grant, D.M. and Harris, R.K. (Eds.), J. Wiley and Sons, London.

Castellani, F., van Rossum, B., Diehl, A., Schubert, M., Rehbein, K. and Oschkinat, H. (2002) *Nature*, **420**, 98–102.

Cornilescu, G., Delaglio, F. and Bax, A. (1999) *J. Biomol. NMR*, **13**, 289–302.

Creemers, A.F.L., Kiihne, S., Bovee-Geurts, P.H.M., DeGrip, W.J., Lugtenburg, J. and de Groot, H.J.M. (2002) *Proc. Natl. Acad. Sci. USA*, **99**, 9101–9106.

Delaglio, F., Grzesiek, S., Vuister, G.W., Zhu, G., Pfeifer, J. and Bax, A. (1995) *J. Biomol. NMR*, **6**, 277–293.

Detken, A., Hardy, E.H., Ernst, M., Kainosho, M., Kawakami, T., Aimoto, S. and Meier, B.H. (2001) *J. Biomol. NMR*, **20**, 203–221.

Deutscher, J., Galinier, A. and Martin-Verstraete, I. (2001) In *Bacillus subtilis and its Closest Relatives: From Genes to Cells*, Sonenschein, A.L., Hoch, J.A. and Losick, R. (Eds.), ASM Press, Washington, pp. 129–150.

Deutscher, J., Kuster, E., Bergstedt, U., Charrier, V. and Hillen, W. (1995) *Mol. Microbiol.*, **15**, 1049–1053.

Egorova-Zachernyuk, T.A., Hollander, J., Fraser, N., Gast, P., Hoff, A.J., Cogdell, R., de Groot, H.J.M. and Baldus, M. (2001) *J. Biomol. NMR*, **19**, 243–253.

Favier, A., Brutscher, B., Blackledge, M., Galinier, A., Deutscher, J., Penin, F. and Marion, D. (2002) *J. Mol. Biol.*, **317**, 131–144.

Fieulaine, S., Morera, S., Poncet, S., Mijakovic, I., Galinier, A., Janin, J., Deutscher, J. and Nessler, S. (2002) *Proc. Natl. Acad. Sci. USA*, **99**, 13437–13441.

Galinier, A., Haiech, J., Kilhoffer, M.C., Jaquinod, M., Stulke, J., Deutscher, J. and Martin-Verstraete, I. (1997) *Proc. Natl. Acad. Sci. USA*, **94**, 8439–8444.

Galinier, A., Kravanja, M., Engelmann, R., Hengstenberg, W., Kilhoffer, M.C., Deutscher, J. and Haiech, J. (1998) *Proc. Natl. Acad. Sci. USA*, **95**, 1823–1828.

Guex, N. and Peitsch, M.C. (1997) *Electrophoresis*, **18**, 2714–2723.

Hediger, S., Meier, B.H. and Ernst, R.R. (1995) *Chem. Phys. Lett.*, **240**, 449–456.

Hohwy, M., Rienstra, C.M., Jaroniec, C.P. and Griffin, R.G. (1999) *J. Chem. Phys.*, **110**, 7983–7992.

Hong, M. (1999) *J. Biomol. NMR*, **15**, 1–14.

Hong, M. and Griffin, R.G. (1998) *J. Am. Chem. Soc.*, **120**, 7113–7114.

Jaroniec, C.P., MacPhee, C.E., Astrof, N.S., Dobson, C.M. and Griffin, R.G. (2002) *Proc. Natl. Acad. Sci. USA*, **99**, 16748–16753.

Johnson, B.A. and Blevins, R.A. (1994) *J. Biomol. NMR*, **4**, 603–614.

Jones, B.E., Dossonnet, V., Kuster, E., Hillen, W., Deutscher, J. and Klevit, R.E. (1997) *J. Biol. Chem.*, **272**, 26530–26535.

Juy, M., Penin, F., Favier, A., Galinier, A., Montserret, R., Haser, R., Deutscher, J. and Böckmann, A. (2003), submitted.

Lange, A., Seidel, K., Verdier, L., Luca, S. and Baldus, M. (2003), submitted.

Luca, S., White, J.F., Sohal, A.K., Filipov, D.V., van Boom, J.H., Grisshammer, R. and Baldus, M. (2003) *Proc. Natl. Acad. Sci. USA*, in press.

Markley, J.L., Bax, A., Arata, Y., Hilbers, C.W., Kaptein, R., Sykes, B.D., Wright, P.E. and Wüthrich, K. (1998) *Eur. J. Biochem.*, **256**, 1–15.

McDermott, A., Polenova, T., Böckmann, A., Zilm, K.W., Paulsen, E.K., Martin, R.W. and Montelione, G.T. (2000) *J. Biomol. NMR*, **16**, 209–219.

Metz, G., Wu, X.L. and Smith, S.O. (1994) *J. Magn. Reson. Ser. A*, **110**, 219–227.

Nielsen, N.C., Bildsoe, H., Jakobsen, H.J. and Levitt, M.H. (1994) *J. Chem. Phys.*, **101**, 1805–1812.

Nomura, K., Takegoshi, K., Terao, T., Uchida, K. and Kainosho, M. (1999) *J. Am. Chem. Soc.*, **121**, 4064–4065.

Pauli, J., Baldus, M., van Rossum, B., de Groot, H. and Oschkinat, H. (2001) *Chembiochemistry*, **2**, 272–281.

Pauli, J., van Rossum, B., Förster, H., de Groot, H.J.M. and Oschkinat, H. (2000) *J. Magn. Reson.*, **143**, 411–416.

Penin, F., Favier, A., Montserret, R., Brutscher, B., Deutscher, J., Marion, D. and Galinier, A. (2001) *J. Mol. Microbiol. Biotechnol.*, **3**, 429–432.

Petkova, A.T., Baldus, M., Belenky, M., Hong, M., Griffin, R.G. and Herzfeld, J. (2003) *J. Magn. Reson.*, **160**, 1–12.

Petkova, A.T., Ishii, Y., Balbach, J.J., Antzutkin, O.N., Leapman, R.D., Delaglio, F. and Tycko, R. (2002) *Proc. Natl. Acad. Sci. USA*, **99**, 16742–16747.

Rienstra, C.M., Hohwy, M., Hong, M. and Griffin, R.G. (2000) *J. Am. Chem. Soc.*, **122**, 10979–10900.

Rienstra, C.M., Hohwy, M., Mueller, L.J., Jaroniec, C.P., Reif, B. and Griffin, R.G. (2002a) *J. Am. Chem. Soc.*, **124**, 11908–11922.

Rienstra, C.M., Tucker-Kellogg, L., Jaroniec, C.P., Hohwy, M., Reif, B., McMahon, M.T., Tidor, B., Lozano-Perez, T. and Griffin, R.G. (2002b) *Proc. Natl. Acad. Sci. USA*, **99**, 10260–10265.

Seavey, B.R., Farr, E.A., Westler, W.M. and Markley, J.L. (1991) *J. Biomol. NMR*, **1**, 217–236.

Straus, S.K., Bremi, T. and Ernst, R.R. (1996) *Chem. Phys. Lett.*, **262**, 709–715.

Straus, S.K., Bremi, T. and Ernst, R.R. (1997) *J. Biomol. NMR*, **10**, 119–128.

Straus, S.K., Bremi, T. and Ernst, R.R. (1998) *J. Biomol. NMR*, **12**, 39–50.

Stulke, J. and Hillen, W. (2000) *Annu. Rev. Microbiol.*, **54**, 849–880.

Tan, W.M., Gu, Z., Zeri, A.C. and Opella, S.J. (1999) *J. Biomol. NMR*, **13**, 337–342.

Verel, R., Baldus, M., Ernst, M. and Meier, B.H. (1998) *Chem. Phys. Lett.*, **287**, 421–428.

Wüthrich, K. (1986) *NMR of Proteins and Nucleic Acids*, Wiley, New York, NY.